

Reconstruction of interaction rate in Holographic dark energy

Ankan Mukherjee ¹

Department of Physical Sciences,
Indian Institute of Science Education and Research Kolkata,
Mohanpur, West Bengal-741246, India

Abstract. The present work is based on the holographic dark energy model with Hubble horizon as the infrared cut-off. The interaction rate between dark energy and dark matter has been reconstructed for three different parameterizations of the deceleration parameter. Observational constraints on the model parameters have been obtained by maximum likelihood analysis using the observational Hubble parameter data (OHD), type Ia supernovae data (SNe), baryon acoustic oscillation data (BAO) and the distance prior of cosmic microwave background (CMB) namely the CMB shift parameter data (CMBShift). The interaction rate obtained in the present work remains always positive and increases with expansion. It is very similar to the result obtained by Sen and Pavon [87] where the interaction rate has been reconstructed for a parametrization of the dark energy equation of state. Tighter constraints on the interaction rate have been obtained in the present work as it is based on larger data sets. The nature of the dark energy equation of state parameter has also been studied for the present models. Though the reconstruction is done from different parametrizations, the overall nature of the interaction rate is very similar in all the cases. Different information criteria and the Bayesian evidence, which have been invoked in the context of model selection, show that these models are at close proximity of each other.

¹E-mail: ankan_ju@iiserkol.ac.in

Contents

1	Introduction	1
2	Reconstruction of the interaction rate	3
3	Observational data	6
3.1	Observational Hubble parameter data	6
3.2	Type Ia supernova data	7
3.3	Baryon acoustic oscillation data	7
3.4	CMB shift parameter data:	8
4	Results of statistical analysis	8
5	Bayesian Evidence and model selection	12
6	Discussion	15

Contents

1 Introduction

The recent cosmic acceleration, discovered in late nineties [1, 2], is presently the most puzzling phenomenon of modern cosmology. It has put a question mark to the basic frame work of cosmology as there is no appropriate answer in the cosmological standard model regarding the genesis of cosmic acceleration. Various observation like the Baryon Oscillation Spectroscopic Survey (BOSS) [3], the continuation of supernova cosmology project [4], the Dark Energy Survey [5], the mapping of the universe from the multi wavelength observations of the Sloan Digital Sky Survey (SDSS) [6], the observation of cosmic microwave background (CMB) from WMAP, Planck [7, 8] etc. are directed towards different aspects of the imprints of evolutions. The basic endeavour is to have a combination of different observations to understand the evolution history and to find the reason behind the cosmic acceleration. The unprecedented improvements in cosmological observations have upgraded the observational data to a higher level of precision and much tighter constraints on various cosmological models have been achieved. But still now, there is hardly any signature to identify the actual reason of cosmic acceleration.

In literature, there are various prescriptions to explain this phenomenon. These can be classified into two classes. One is the *dark energy*, an exotic component introduced in the energy budget of the universe, which can generate the cosmic acceleration with its characteristic negative pressure. For the dark energy models, the General Relativity (GR) is taken as the proper theory of gravity. The other way to look for the solution through the modification of GR such as $f(R)$ gravity models [9–17], scalar-tensor theory [18–24], different higher dimensional gravity theories [25–30] etc.

In the context of dark energy, the simplest and consistent with most of the observations is the cosmological constant model where the constant vacuum energy density serves as the dark energy candidate. But there are different issues related to the cosmological constant model. There is a huge

discrepancy between the observationally estimated value of cosmological constant and the value calculated from quantum field theory. It also suffers from the cosmic coincidence problem. Comprehensive discussions on the cosmological constant model are there by Carroll [31] and by Padmanabhan [32] where different issues have been emphasised in great details. Due to these issues related to the cosmological constant, time varying dark energy models also warrant attention. Review articles with comprehensive discussion on different dark energy models are there in literature [33–36]. The present trend in cosmological modelling is *reconstruction* which is a reverse way of finding the viable model of cosmic evolution. The idea is to adopt a viable evolution scenario and then to find the behaviour of the relevant cosmological quantities and to estimate the values of the parameters associated to the model. Reconstruction of dark energy models has earlier been discussed by Starobinsky [37], Huterer and Turner [38, 39] and by Saini et al. [40]. With the recent unprecedented improvement in the cosmological observations, the dark energy models are becoming highly constrained. Parametric and non-parametric, both types of reconstructions with various updated observational data are giving more and more precise estimation of the dark energy parameters [41–45]. Reconstruction of kinematical quantities like the deceleration parameter, cosmological jerk parameter have been discussed in reference [46–49].

In most of the dark energy models, the dark matter and dark energy are allowed to have independent conservation, ignoring the possibility of interaction between them. Das *et al.* [50] and Amendola *et al.* [51] have shown that the prior ignorance of the interaction between the dark energy and dark matter might cause some misleading results. It has been argued that the phantom nature of dark energy might be consequence of ignoring the possibility of interaction between dark energy and dark matter [50, 51]. There are also good number of investigations in the literature on the interacting dark energy models [52–57]. Interaction between Brans-Dicke scalar field and quintessence has been discussed by Banerjee and Das [58]. Some recent attempts to find the constraint on interacting dark energy models from recent observational data are by Paliathanasis and Tsamparlis [59], by Pan *et al.* [60], Nunes *et al.* [61] and by Murgia *et al.* [62]. In a recent analysis by Salvatelli *et al.* [63], it has been shown that an interacting vacuum cosmology, where the coupling strength varies with redshift, can be a possible solution to the tension in Λ CDM model between the CMB data and the measurement of linear growth rate of large scale structure (LSS) from redshift-space distortion (RSD) data. Non-parametric reconstruction of interacting dark energy has been discussed by Yang *et al.* [64]. Recent review on dark matter dark energy interaction by Wang *et al.* [65] presents a comprehensive discussion on different aspects and theoretical challenges of interacting dark energy.

The present work is the reconstruction of the interaction rate of *holographic dark energy*. The basic idea of holographic dark energy is based on fundamental thermodynamic consideration, namely the *holographic principal*, introduced by 't Hooft [66] and Susskind [67]. To avoid the violation of the second law of thermodynamics in the context of quantum theory of gravity, Bekenstein suggested that the maximum entropy of the system should be proportional to its area instead of its volume [68]. From this idea, 't Hooft conjectured that the phenomena within a volume can be explained by the set of degrees of freedom residing on its boundary and the degrees of freedom of a system is determined by the area of the boundary instead of the volume of the system. In quantum field theory it relates a short distance cut-off (ultraviolet (UV) cut-off) to a long distance cut off (infra red (IR) cut-off) in the limit set by the formation of a black hole [69]. The total quantum zero point energy of a system should not exceed the mass of a black hole of the same size. If ρ_Λ be the quantum zero point energy density caused by the short distance cut-off, the total energy is $L^3\rho_\Lambda$, where L is the size of the system. Thus it can be written as [70],

$$L^3\rho_\Lambda \leq LM_P^2, \quad (1.1)$$

where $M_P^2 = (8\pi G)^{-1}$. The inequality saturates for the largest allowed value of the system size L , which is the long distance cut-off or the infrared cut-off. Thus the energy density ρ_Λ be proportional to inverse square of the infra red cut-off. This idea have been adopted in the context of dark energy by Li [70]. Thus the holographic dark energy density is written as,

$$\rho_H = 3C^2 M_P^2 / L^2, \quad (1.2)$$

where C^2 is a dimensionless constant. Different attempts are there in literature with different selections of the infrared cut-off length scale, the particle horizon [71, 72], the future event horizon [70, 73–78] and the Hubble horizon [79] etc. Holographic dark energy in Brans-Dicke theory has been discussed by Banerjee and Pavon [81]. Xu has studied holographic dark energy with the Hubble horizon cut-off with constant as well as time varying coupling parameter (C^2) [82]. A comparative study of the holographic dark energy with different length scale cut-off has been carried out by Campo *et al.* [83]. Recently Hu *et al.* [84] has attempted to built up the model combining cosmological constant and holographic energy density. Holographic dark energy from minimal supergravity has been discussed by Landim [85]. Stability analysis of holographic dark energy model has been discussed by Banerjee and Roy [86].

In the present work, the Hubble horizon has been adopted as the infrared cut-off for the holographic dark energy meaning the cutoff length scale $L = (H)^{-1}$, where H is the Hubble parameter. Now it is imperative to note that the holographic dark energy models with Hubble horizon cut off can generate late time acceleration along with the matter dominated decelerated expansion phase in the past only if there is some interaction between dark energy and dark mater.

In the present work, the interaction rate of holographic dark energy has been reconstructed from three different parameterizations of the deceleration parameter. The expressions of Hubble parameter obtained for these models hardly give any indication towards the independent conservation of dark matter and dark energy. The prime endeavour of the present work is to study the nature of interaction and the evolution of the interaction rate for these three models assuming the holographic dark energy with Hubble horizon as the IR cut-off. Reconstruction of interaction rate in holographic dark energy has earlier been discussed by Sen and Pavon [87], where the interaction rate has been reconstructed assuming a particular form of the dark energy equation of state.

In section 2, the reconstruction of the interaction rate for these three models have been discussed. In section 3, a brief discussion about the observational data sets, used in the statistical analysis, have been presented. Section 4 presents the results of statistical analysis of the models including the constraints on the model parameters and also the constraints on the evolution of holographic interaction rate. In section 5, a Bayesian analysis has been presented to select the preferred model among these three, discussed in the present work. Finally, in section 6, an overall discussion about the results obtained has been presented.

2 Reconstruction of the interaction rate

The metric of a homogeneous and isotropic universe with a spatially flat geometry is written as,

$$ds^2 = -dt^2 + a^2(t)[dr^2 + r^2 d\Omega^2], \quad (2.1)$$

where $a(t)$, the time dependent coefficient of the spatial part of the metric, is called the *scale factor*. Now the Hubble parameter is defined as $H = \frac{\dot{a}}{a}$, where the dot denotes the derivative with respect to time. The Friedmann equations, written in terms of H , are

$$3H^2 = 8\pi G(\rho_m + \rho_{DE}), \quad (2.2)$$

and

$$2\dot{H} + 3H^2 = -8\pi G(p_{DE}), \quad (2.3)$$

where ρ_m is the energy density of the pressureless dust matter and ρ_{DE} and p_{DE} are respectively the energy density and pressure of the dark energy. Now from contracted Bianchi identity, the conservation equation can be written as,

$$\dot{\rho}_{total} + 3H(\rho_{total} + p_{total}) = 0, \quad (2.4)$$

where $\rho_{total} = \rho_m + \rho_{DE}$ and $p_{total} = p_{DE}$ as the dark matter is pressureless. Now the conservation equation (equation 2.4) can be decomposed into two parts,

$$\dot{\rho}_m + 3H\rho_m = Q, \quad (2.5)$$

and

$$\dot{\rho}_{DE} + 3H(1 + w_{DE})\rho_{DE} = -Q, \quad (2.6)$$

where w_{DE} is the equation of state parameter of dark energy and the Q is the interaction term. If there is no interaction between dark energy and dark matter, then the interaction term $Q = 0$, and the matter evolves as, $\rho_m \propto \frac{1}{a^3}$.

The prime goal of the present work is to study the interaction assuming a holographic dark energy with Hubble horizon as the IR cut off. Holographic dark energy models with the Hubble horizon H^{-1} as the IR cut-off require the interaction between the dark energy and dark matter to generate the late time acceleration. The dark energy density ρ_{DE} for a holographic model with the Hubble horizon as the IR cut-off (denoted as ρ_H) is given, according to equation (1.2) as,

$$\rho_H = 3C^2 M_P^2 H^2, \quad (2.7)$$

where C , the coupling parameter is assumed to be a constant in the present work and $M_P = \frac{1}{\sqrt{8\pi G}}$. Now the interaction term Q is written as, $Q = \rho_H \Gamma$, where Γ is the rate at which the energy exchange occurs between dark energy and dark matter. The ratio of dark matter and dark energy density, sometimes called the *coincidence parameter*, is written as, $r = \rho_m / \rho_H$, and its time derivative can be expressed as [87],

$$\dot{r} = (1 + r) \left[3Hw_{DE} \frac{r}{1 + r} + \Gamma \right]. \quad (2.8)$$

For a spatially flat geometry, it can also be shown that the ratio r remains constant for a holographic dark energy with Hubble horizon as the IR cut-off. As the ratio of dark matter and dark energy remains constant in this case, it can potentially convey the answer to the cosmic coincidence problem. But it might be confusing as one may think that it contradicts the standard scenario of structure formation during the dark matter dominated epoch. Actually this is not the case. The matter dominated phase is automatically recovered as the interaction rate is very small at high and moderate redshift and thus the dark energy equation of state resembles the non-relativistic matter [79, 80]. For a constant value of r , $\dot{r} = 0$, from which the interaction rate can be expressed using equation (2.8) as,

$$\Gamma = -3Hr \frac{w_{DE}}{1 + r}. \quad (2.9)$$

The effective or total equation of state parameter ($w_{eff} = \frac{p_{total}}{\rho_{total}}$), is related to the dark energy equation of state parameter as,

$$w_{eff} = \frac{w_{DE}}{1 + r}. \quad (2.10)$$

Finally the interaction can be written as,

$$\Gamma = -3Hrw_{eff}, \quad (2.11)$$

and representing it in a dimensionless way,

$$\frac{\Gamma}{3H_0} = -(H/H_0)rw_{eff}. \quad (2.12)$$

In the present work, the interaction rate has been reconstructed for three different parameterizations of the deceleration parameter. The expression of the Hubble parameter obtained for these models hardly give any indication of the independent evolution of dark energy and dark matter, thus these parameterizations are useful to study the interaction. These parameterizations of deceleration parameter have been discussed in the following. It worth mentioning that for the reconstruction of the interaction rate, it is required to fix the value of the coincident parameter r . The value of r is taken according to the recent measurement of the dark energy density parameter Ω_{DE0} from Planck using Planck+WP+highL+BAO [88] as for spatially flat universe r can be written as $r = (1 - \Omega_{DE0})/\Omega_{DE0}$. It is imperative to note that the interaction rate Γ does not depends upon the coupling parameter (C^2). The effective equation of state parameter ($w_{eff}(z)$) can be obtained from the Hubble parameter using the Friedmann equations (equation (2.2) and (2.3)).

The deceleration parameter, a dimensionless representation of the second order time derivative of the scale factor, is defined as $q = -\frac{1}{H^2} \frac{\ddot{a}}{a}$. It can also be written using redshift z as the argument of differentiation as,

$$q(z) = -1 + \frac{1}{2}(1+z) \frac{(H^2)'}{H^2}. \quad (2.13)$$

The parametric forms of the deceleration parameter, adopted in the present work, are given as,

$$\text{Model I.} \quad q(z) = q_1 + \frac{q_2}{(1+z)^2}, \quad (2.14)$$

$$\text{Model II.} \quad q(z) = \frac{1}{2} + \frac{q_1 + q_2 z}{(1+z)^2}, \quad (2.15)$$

$$\text{Model III.} \quad q(z) = -1 + \frac{q_1(1+z)^2}{q_2 + (1+z)^2}, \quad (2.16)$$

where q_1 and q_2 are the parameters for the models. However, q_1 and q_2 do not have the same physical significance in the three different models. The second model of deceleration parameter adopted in the present work has already been discussed by Gong and Wang [89, 90] in the context of reconstruction of the late time dynamics of the Universe. The parametrization of Model III has some similarity with one of the parametrizations based on thermodynamic requirement discussed by Campo *et al.* [91]. The variation of deceleration parameter at low redshift is higher for Model I and Model II than Model III. Thus parametrization of Model III is significantly different from other two. The expressions of Hubble parameter scaled by its present value for the models yield to be

$$\text{Model I.} \quad h^2(z) = \frac{H^2(z)}{H_0^2} = (1+z)^{2(1+q_1)} \exp \left[-q_2 \left(\frac{1}{(1+z)^2} - 1 \right) \right], \quad (2.17)$$

$$\text{Model II.} \quad h^2(z) = \frac{H^2(z)}{H_0^2} = (1+z)^3 \exp \left[\frac{q_2 - q_1}{(1+z)^2} - \frac{2q_2}{(1+z)} + (q_1 + q_2) \right], \quad (2.18)$$

$$\text{Model III. } h^2(z) = \frac{H^2(z)}{H_0^2} = \left(\frac{q_2 + (1+z)^2}{1+q_2} \right)^{q_1}, \quad (2.19)$$

and consequently the effective equation of state parameter ($w_{eff}(z)$) for the models are expressed as

$$\text{Model I. } w_{eff}(z) = -1 + \frac{2}{3} \left[(1+q_1) + \frac{q_2}{(1+z)^2} \right], \quad (2.20)$$

$$\text{Model II. } w_{eff}(z) = -1 + \frac{1}{3} \left[3 + \frac{2q_2}{(1+z)} - \frac{2(q_2 - q_1)}{(1+z)^2} \right], \quad (2.21)$$

$$\text{Model III. } w_{eff}(z) = -1 + \frac{2}{3} \left(\frac{q_1(1+z)^2}{q_2 + (1+z)^2} \right). \quad (2.22)$$

Utilizing the expression of the effective equation of state, the interaction rate of holographic dark energy can be reconstructed using equation (2.12). It is also worth mentioning in the context is that this expressions of Hubble parameter (equation (2.17), (2.18) and (2.19)) hardly give any indication regarding the independent conservation of dark matter and dark energy as the dark matter and dark energy components are not separately identified in the expressions of $h^2(z)$ in equations (2.17), (2.18) and (2.19).

3 Observational data

Different observational data sets have been utilized for the statistical analysis of the models in the present work. These are the observational Hubble data (OHD), distance modulus data from type Ia supernove (SNe), baryon acoustic oscillation (BAO) data along with the value of acoustic scale at photon electron decoupling and the ratio of comoving sound horizon at decoupling and at drag epoch estimated from Cosmic Microwave Background (CMB) radiation power spectrum and the CMB distance prior namely the CMB shift parameter (CMBShift) data. The data sets are briefly discussed in the following. The discussion about the observational data has also been presented in a very similar fashion in [45, 49]

3.1 Observational Hubble parameter data

The data of Hubble parameter measurement by different groups have been used in the present analysis. Hubble parameter $H(z)$ can be estimated from the measurement of differential of redshift z with respect to cosmic time t as

$$H(z) = -\frac{1}{(1+z)} \frac{dz}{dt}. \quad (3.1)$$

The differential age of galaxies have been used as an estimator of dz/dt by Simon *et al.* [92]. Measurement of cosmic expansion history using red-enveloped galaxies was done by Stern *et al* [93] and by Chuang and Wang [94]. Measurement of expansion history from WiggleZ Dark Energy Survey has been discussed by Blake *et al.* [96]. Measurement of Hubble parameter at low redshift using the differential age method along with Sloan Digital Sky Survey (SDSS) data have been presented by Zhang *et al* [97]. Compilation of observational Hubble parameter measurement has been presented by Moresco *et al* [95]. Finally, the measurement of Hubble parameter at $z = 2.34$ by Delubac *et al* [98] has also been used in the present analysis. The measurement of H_0 from Planck+WP+highL+BAO [88] has also been used in the analysis. The relevant χ^2 is defined as

$$\chi_{OHD}^2 = \sum_i \frac{[H_{obs}(z_i) - H_{th}(z_i, \{\theta\})]^2}{\sigma_i^2}, \quad (3.2)$$

where H_{obs} is the observed value of the Hubble parameter, H_{th} is theoretical one and σ_i is the uncertainty associated to the i^{th} measurement. The χ^2 is a function of the set of model parameters $\{\theta\}$.

3.2 Type Ia supernova data

The measurement of the distance modulus of type Ia supernova of the most widely used data set in the modelling of late time cosmic acceleration. The distance modulus of type Ia supernova is the difference between the apparent magnitude (m_B) and absolute magnitude (M_B) of the B-band of the observed spectrum. It is defined as

$$\mu(z) = 5 \log_{10} \left(\frac{d_L(z)}{1 \text{ Mpc}} \right) + 25, \quad (3.3)$$

where the $d_L(z)$ is the luminosity distance and in a spatially flat FRW universe it is defined as

$$d_L(z) = (1+z) \int_0^z \frac{dz'}{H(z')}. \quad (3.4)$$

In the present work, the 31 binned data sample of the recent joint lightcurve analysis (jla) [99] has been utilized. To account for the correlation between different bins, The formalism discussed by Farooq, Mania and Ratra [100] to account for the correlation between different redshift bins, has been adopted. The χ_{SNe}^2 has been defined as

$$\chi_{SNe}^2 = A(\{\theta\}) - \frac{B^2(\{\theta\})}{C} - \frac{2 \ln 10}{5C} B(\{\theta\}) - Q, \quad (3.5)$$

where

$$A(\{\theta\}) = \sum_{\alpha, \beta} (\mu_{th} - \mu_{obs})_{\alpha} (Cov)_{\alpha\beta}^{-1} (\mu_{th} - \mu_{obs})_{\beta}, \quad (3.6)$$

$$B(\{\theta\}) = \sum_{\alpha} (\mu_{th} - \mu_{obs})_{\alpha} \sum_{\beta} (Cov)_{\alpha\beta}^{-1}, \quad (3.7)$$

$$C = \sum_{\alpha, \beta} (Cov)_{\alpha\beta}^{-1}, \quad (3.8)$$

and the Cov is the 31×31 covariance matrix of the binning. The constant term Q can be ignored during the analysis as it is independent of the model parameters.

3.3 Baryon acoustic oscillation data

The baryon acoustic oscillation (BAO) data have been used in the present analysis in combination with the Planck [88, 103] measurement of the *acoustic scale* (l_A), the *comoving sound horizon* (r_s) at photon decoupling epoch (z_*) and at drag epoch (z_d). The BAO data have been used in the form of a ratio of the *comoving angular diameter distance* at decoupling ($d_A(z_*) = c \int_0^{z_*} \frac{dz'}{H(z')}$), and the *dilation scale* ($D_V(z) = [czd_A^2(z)/H(z)]^{\frac{1}{3}}$). Three mutually uncorrelated measurements of $\frac{r_s(z_d)}{D_V(z)}$ (6dF Galax Survey at redshift $z = 0.106$ [101], Baryon Oscillation Spectroscopic Survey (BOSS) at redshift $z = 0.32$ (BOSS LOWZ) and at redshift $z = 0.57$ (BOSS CMASS) [102]) have been adopted in the present analysis. Table 1 contains the values of $\left(\frac{r_s(z_d)}{D_V(z_{BAO})} \right)$ and finally the $\left(\frac{d_A(z_*)}{D_V(z_{BAO})} \right)$ at three different redshift of BAO measurement.

Table 1. BAO/CMB data table

z_{BAO}	0.106	0.32	0.57
$\frac{r_s(z_d)}{D_V(z_{BAO})}$	0.3228 ± 0.0205	0.1167 ± 0.0028	0.0718 ± 0.0010
$\frac{d_A(z_*)}{D_V(z_{BAO})} \frac{r_s(z_d)}{r_s(z_*)}$	31.01 ± 1.99	11.21 ± 0.28	6.90 ± 0.10
$\frac{d_A(z_*)}{D_V(z_{BAO})}$	30.43 ± 2.22	11.00 ± 0.37	6.77 ± 0.16

The relevant χ^2 , namely χ_{BAO}^2 , is defined as:

$$\chi_{BAO}^2 = \mathbf{X}^t \mathbf{C}^{-1} \mathbf{X}, \quad (3.9)$$

where

$$\mathbf{X} = \begin{pmatrix} \frac{d_A(z_*)}{D_V(0.106)} - 30.43 \\ \frac{d_A(z_*)}{D_V(0.2)} - 11.00 \\ \frac{d_A(z_*)}{D_V(0.35)} - 6.77 \end{pmatrix}$$

and \mathbf{C}^{-1} is the inverse of the covariance matrix. As the three measurements are mutually uncorrelated, the covariance matrix is diagonal.

3.4 CMB shift parameter data:

The CMB shift parameter, which is related to the position of the first acoustic peak in power spectrum of the temperature anisotropy of the Cosmic Microwave Background (CMB) radiation, is defined in a spatially flat universe as,

$$\mathcal{R} = \sqrt{\Omega_{m0}} \int_0^{z_*} \frac{dz}{h(z)}, \quad (3.10)$$

where Ω_{m0} is the matter density parameter, z_* is the redshift at photon decoupling and $h(z) = \frac{H(z)}{H_0}$ (where H_0 be the present value of Hubble parameter). In general it is efficient to ensure tighter constraints on the model parameters if used in combination with other observational data. The value of CMB shift parameter is not directly measured from CMB observation. The value is estimated from the CMB data along with some fiducial assumption about the background cosmology. The $\chi_{CMBShift}^2$ is defined as

$$\chi_{CMBShift}^2 = \frac{(\mathcal{R}_{obs} - \mathcal{R}_{th}(z_*))^2}{\sigma^2}, \quad (3.11)$$

where \mathcal{R}_{obs} is the value of the CMB shift parameter, estimated from observation and σ is the corresponding uncertainty. In this work, the value of CMB shift parameter estimated from Planck data [103] has been used. It is imperative to mention that in the present analysis the value Ω_{m0} is taken according to recent estimation from Planck [88].

4 Results of statistical analysis

An indispensable part of reconstruction is the estimation of the values of the model parameters from observational data. The values of the model parameters have been estimated by χ^2 minimization. Normally the χ^2 is defined as

$$\chi^2(\{\theta\}) = \sum_i \frac{[\epsilon_{obs}(z_i) - \epsilon_{th}(z_i, \{\theta\})]^2}{\sigma_i^2}, \quad (4.1)$$

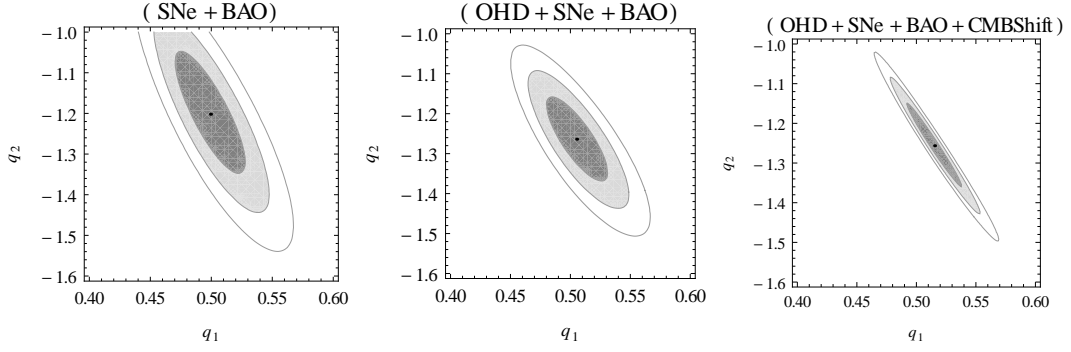


Figure 1. The confidence contours on the 2D parameter space of Model I. The 1σ , 2σ , and 3σ confidence contours are presented from inner to outer regions, and the central black dots represent the corresponding best fit points. The left panel is obtained for SNe+BAO, the middle panel is obtained for OHD+SNe+BAO and the right panel is for OHD+SNe+BAO+CMBShift.

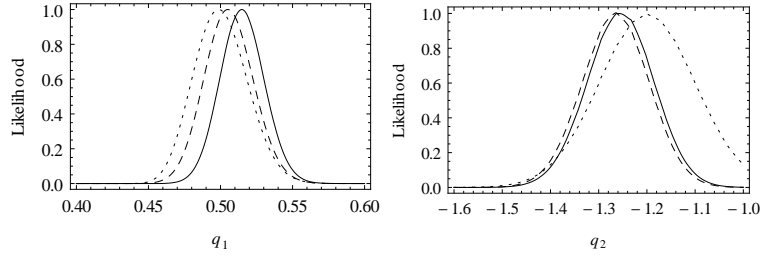


Figure 2. The marginalized likelihood as function of the model parameters q_1 (left panel) and q_2 (right panel) for Model I. The dotted curves are obtained for SNe+BAO, the dashed curves are obtained for OHD+SNe+BAO and the solid curves are obtained for OHD+SNe+BAO+CMBShift.

where ϵ_{obs} is the value of the observable measured at redshift z_i , ϵ_{th} from of the observable quantity as a function of the set of model parameters $\{\theta\}$ and σ_i is the uncertainty associated to the measurement at z_i . In case of supernova distance modulus data and BAO data, the relevant χ^2 are defined in a complicated way to incorporate the associated correlation matrix (equations (3.5) and (3.9)). The combined analysis has been carried out by adding the χ^2 of the individual data sets taken into account for that particular combination. The combined χ^2 is defined as,

$$\chi_{combined}^2 = \sum_d \chi_d^2, \quad (4.2)$$

where d represents the individual data set. The χ^2 associated to different data sets have been discussed in section 3.

The χ^2 minimization, which is equivalent to the maximum likelihood analysis, has been adopted in the present work for the estimation of the parameter values. The likelihood is defined as,

$$\mathcal{L}(\{\theta\}) = \exp\left(-\frac{\chi^2}{2}\right). \quad (4.3)$$

Figure 1 shows the confidence contours on the 2D parameter space of Model I obtained from analysis with different combinations of the data sets. Figure 2 shows the plots of the marginalized

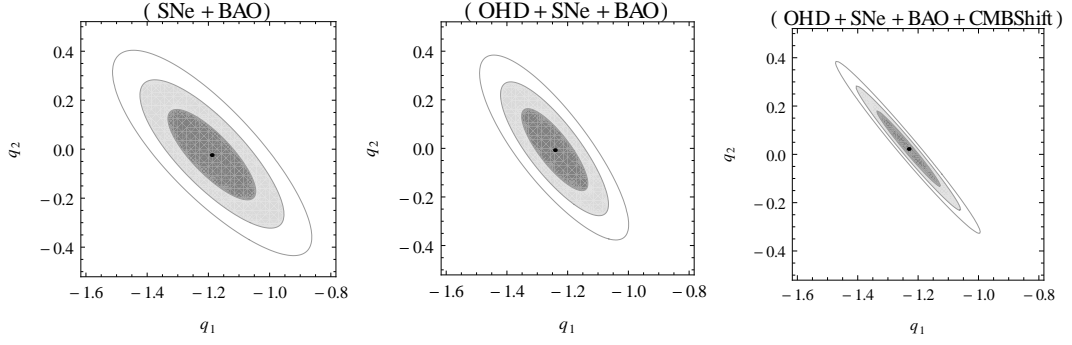


Figure 3. The confidence contours on the 2D parameter space of Model II. The 1σ , 2σ , and 3σ confidence contours are presented from inner to outer regions, and the central black dots represent the corresponding best fit points. The left panel is obtained for SNe+BAO, the middle panel is obtained for OHD+SNe+BAO and the right panel is for OHD+SNe+BAO+CMBShift.

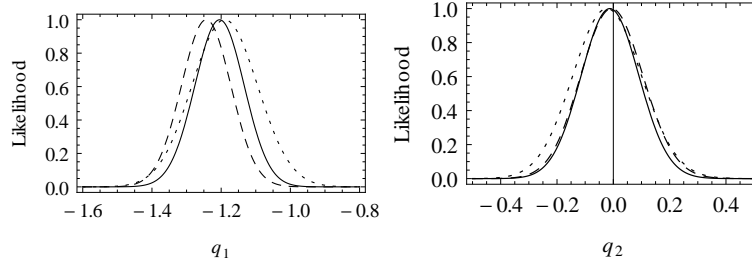


Figure 4. The marginalized likelihood as function of the model parameters q_1 (left panel) and q_2 (right panel) for Model II. The dotted curves are obtained for SNe+BAO, the dashed curves are obtained for OHD+SNe+BAO and the solid curves are obtained for OHD+SNe+BA+CMBShift.

Table 2. Results of statistical analysis of Model I with different combinations of the data sets. The value of $\chi^2_{min}/d.o.f.$ and the best fit values of the parameters along with the associated 1σ uncertainties are presented.

Data	$\chi^2_{min}/d.o.f.$	q_1	q_2
SNe+BAO	35.18/28	0.499 ± 0.051	-1.202 ± 0.367
OHD+SNe+BAO	50.57/54	0.505 ± 0.014	-1.264 ± 0.064
OHD+SNe+BAO+CMBShift	51.97/52	0.515 ± 0.013	-1.256 ± 0.062

Table 3. Results of statistical analysis of Model II with different combinations of the data sets. The value of $\chi^2_{min}/d.o.f.$ and the best fit values of the parameters along with the associated 1σ uncertainties are presented.

Data	$\chi^2_{min}/d.o.f.$	q_1	q_2
SNe+BAO	35.18/28	-1.189 ± 0.067	-0.024 ± 0.086
OHD+SNe+BAO	50.64/54	-1.242 ± 0.050	-0.007 ± 0.078
OHD+SNe+BAO+CMBShift	51.17/52	-1.231 ± 0.049	0.022 ± 0.073

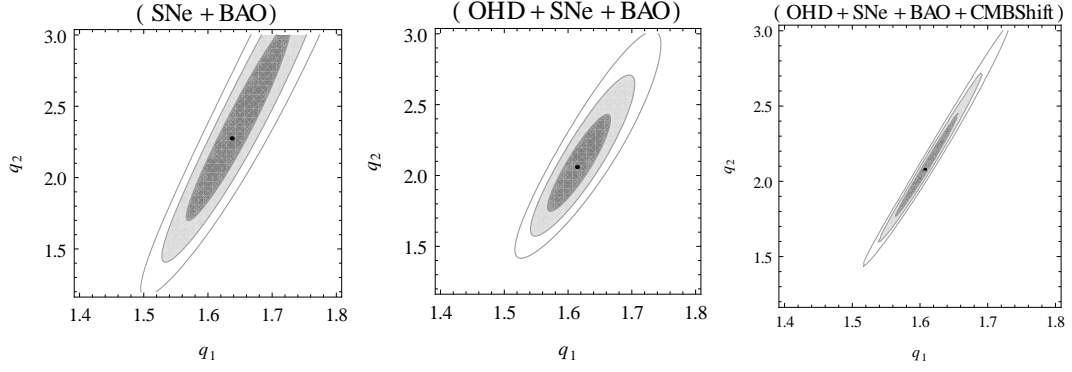


Figure 5. The confidence contours on the 2D parameter space of Model III. The 1σ , 2σ , and 3σ confidence contours are presented from inner to outer regions, and the central black dots represent the corresponding best fit points. The left panel is obtained for SNe+BAO, the middle panel is obtained for OHD+SNe+BAO and the right panel is for OHD+SNe+BAO+CMBShift.

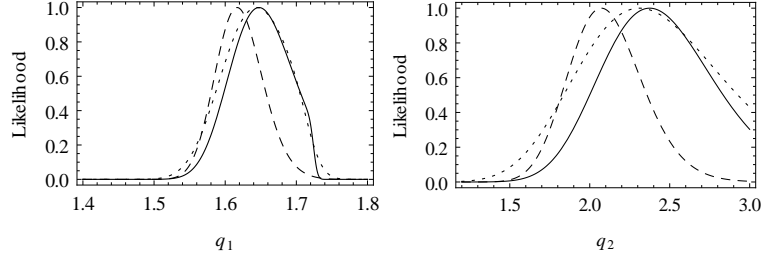


Figure 6. The marginalized likelihood as function of the model parameters q_1 (left panel) and q_2 (right panel) for Model III. The dotted curves are obtained for SNe+BAO, the dashed curves are obtained for OHD+SNe+BAO and the solid curves are obtained for OHD+SNe+BA+CMBShift.

Table 4. Results of statistical analysis of Model III with different combinations of the data sets. The value of $\chi^2_{min}/d.o.f.$ and the best fit values of the parameters along with the associated 1σ uncertainties are presented.

Data	$\chi^2_{min}/d.o.f.$	q_1	q_2
SNe+BAO	33.18/28	1.637 ± 0.037	2.275 ± 0.315
OHD+SNe+BAO	47.80/54	1.614 ± 0.023	2.059 ± 0.162
OHD+SNe+BAO+CMBShift	48.31/52	1.607 ± 0.022	2.079 ± 0.160

likelihood as functions of the model parameters for Model I. Similarly, figure 3 shows the confidence contours on the 2D parameter space of Model II and figure 4 shows the marginalized likelihoods of Model II. Figure 5 and figure 6 present contour plots and likelihood plots respectively for Model III. It is apparent from the contour plots and the likelihood function plots that the addition of the CMB shift parameter data does not lead to much improvement of the constraints on the model parameters. The likelihood functions are well fitted to Gaussian distribution. Table 2 presents the results of statistical analysis of Model I. The reduced χ^2 i.e. $\chi^2_{min}/d.o.f.$, where the *d.o.f.* is the degrees of freedom associated to the analysis, the best fit values of the parameters along with the associated 1σ error bars

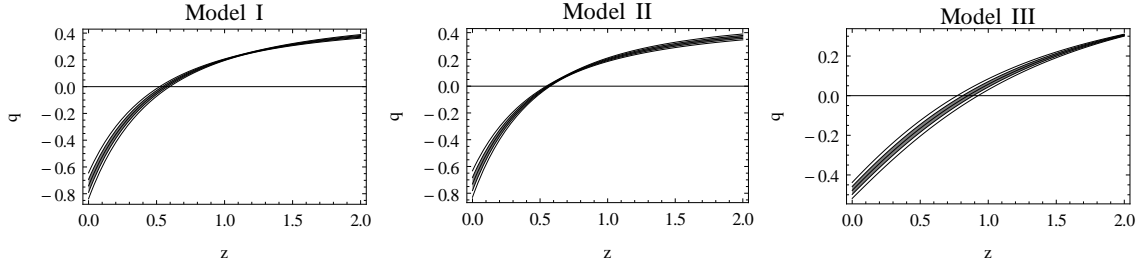


Figure 7. Plots of deceleration parameter for the models obtained from the analysis combining OHD, SNe, BAO and CMB shift parameter data. The best fit curve and the associated 1σ and 2σ confidence regions are presented.

are presented. In the similar way, table 3 and table 4 present the results of the statistical analysis of Model II and Model III respectively. Figure 7 shows the plots of deceleration parameter for the models obtained in the combined analysis with OHD, SNe, BAO and CMB shift parameter data.

The plots of the interaction rate ($\Gamma(z)/3H_0$) (figure 8, figure 9 and figure 10) show that the interaction was low at earlier and it increases significantly at recent time. For Model I and Model III, the nature of constraint on the interaction rate, obtained in the analysis combining OHD, SNe, BAO and CMB shift data, is similar at present time and also at high redshift. But for Model II, the uncertainty increases at high redshift.

The plots of the dark energy equation of state parameter $w_{DE}(z)$ also shows a very similar behaviour for the models, (figure 11, figure 12 and figure 13). It is imperative to note that for Model I and Model II, the dark energy equation of state parameter indicates a phantom nature at present as $w_{DE}(z=0) < -1$ at 2σ confidence level and for Model III, it is slightly inclined towards the non-phantom nature. At high redshift, the value of $w_{DE}(z)$ be close to zero and thus allows a matter dominated epoch in the recent past.

The interaction rate $\Gamma(z)$ remains positive throughout the evolution and increases with the expansion of the Universe. As the interaction term Q is assumed to be $Q = \rho_H \Gamma$, Q is also positive. This reveals that in the interaction, the energy transfers from dark energy to dark matter. It is consistent with the thermodynamic requirement of a positive Q [104]. It is imperative to note that though the parametrization for Model III is significantly different from Model I and Model II, the basic nature of the interaction rate is same in all the case. Similar results have been obtained by Sen and Pavon [87] where the interaction rate of holographic dark energy has been reconstructed from a parametrization of dark energy equation of state parameter. Though tighter constraints have been achieved in the present work as it is based on larger data sets, the basic nature of the interaction rate shows no deviation from the previous findings.

5 Bayesian Evidence and model selection

In the present work, three models of holographic dark energy have been discussed. It is important to look for the preferred model among these three. Two commonly used information criteria for model selection are Akaike Information Criterion (AIC) [105] and Bayesian Information Criterion (BIC) [106]. They are defined as,

$$AIC = -2 \log \mathcal{L}_{max} + 2\kappa, \quad (5.1)$$

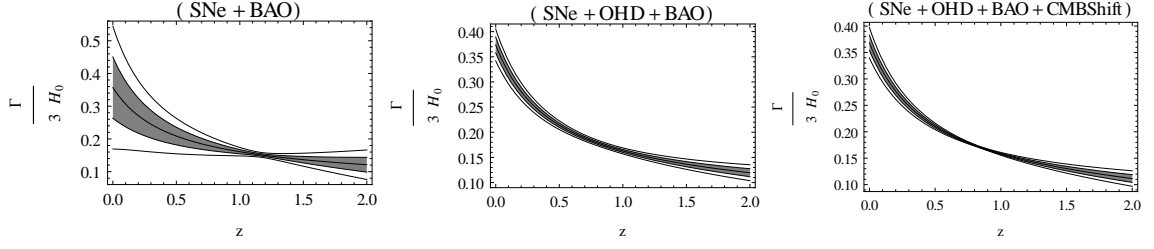


Figure 8. The plots of interaction rate $\Gamma(z)$ scaled by $3H_0$ for Model I. Plots are obtained for three different combinations of the data sets. The left panel is obtained for SNe+BAO, the middle panel is obtained for OHD+SNe+BAO and the right panel is obtained for OHD+SNe+BAO+CMBSHIFT. The 1σ and 2σ confidence regions and the corresponding best fit curves (the central dark line) are shown.

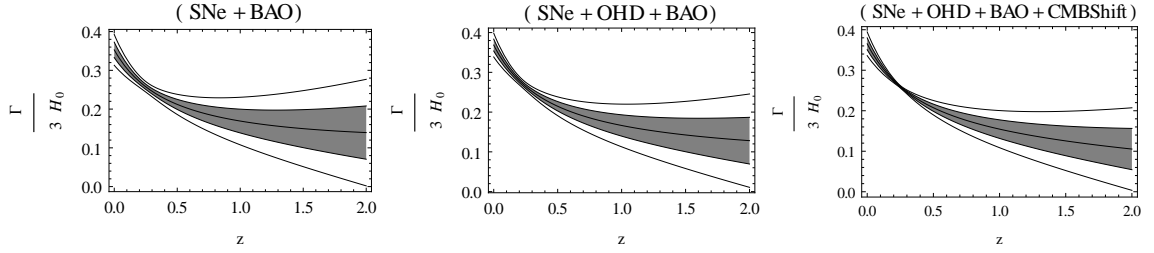


Figure 9. The plots of interaction rate $\Gamma(z)$ scaled by $3H_0$ for Model II. Plots are obtained for three different combinations of the data sets. The left panel is obtained for SNe+BAO, the middle panel is obtained for OHD+SNe+BAO and the right panel is obtained for OHD+SNe+BAO+CMBSHIFT. The 1σ and 2σ confidence regions and the corresponding best fit curves (the central dark line) are shown.

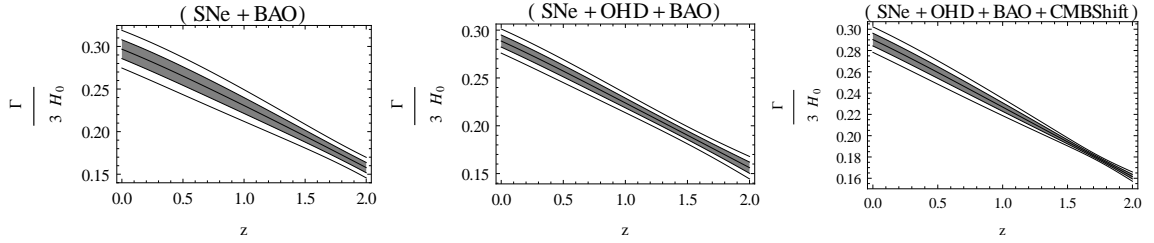


Figure 10. The plots of interaction rate $\Gamma(z)$ scaled by $3H_0$ for Model III. Plots are obtained for three different combinations of the data sets. The left panel is obtained for SNe+BAO, the middle panel is obtained for OHD+SNe+BAO and the right panel is obtained for OHD+SNe+BAO+CMBSHIFT. The 1σ and 2σ confidence regions and the corresponding best fit curves (the central dark line) are shown.

and

$$BIC = -2 \log \mathcal{L}_{max} + 2\kappa \log N, \quad (5.2)$$

where \mathcal{L}_{max} is the maximum likelihood, κ is the number of free parameter, N is the number of data points used in the analysis. In the present work, all the models have two free parameters and same number of data points have been used in the analysis of the models. The difference between AIC of two models, written as ΔAIC and difference between BIC of two models, written as ΔBIC , are actually the difference between the χ^2_{min} of the models. Results obtained from the analysis combining

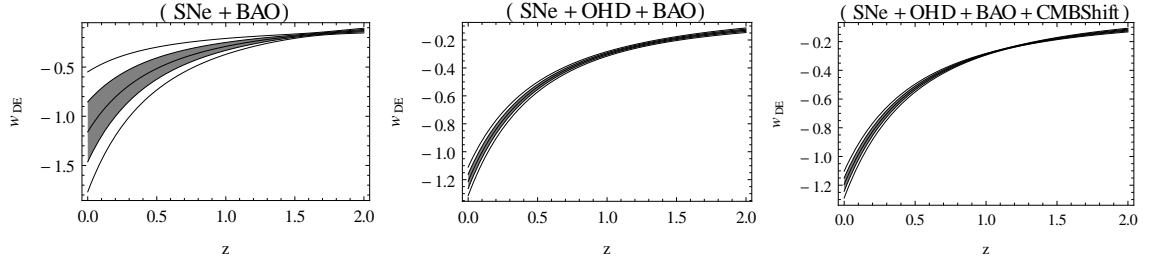


Figure 11. The plots of dark energy equation of state parameter $w_{DE}(z)$ for Model I. The left panel is obtained for SNe+BAO, the middle panel is obtained for OHD+SNe+BAO and the right panel is obtained for OHD+SNe+BAO+CMBShift. The 1σ and 2σ confidence regions and the corresponding best fit curves (the central dark line) are shown.

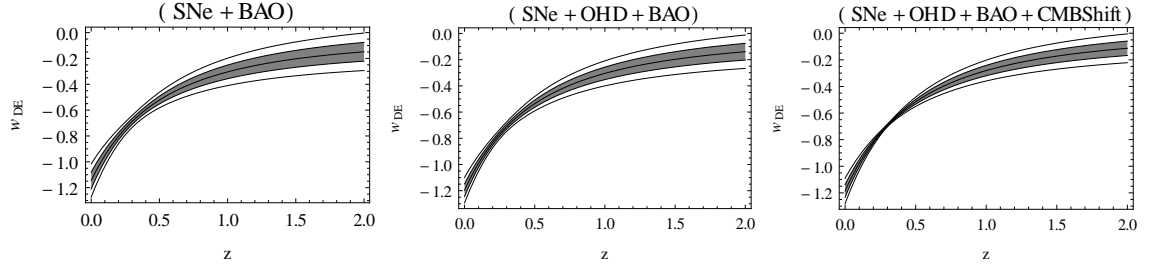


Figure 12. The plots of dark energy equation of state parameter $w_{DE}(z)$ for Model II. The left panel is obtained for SNe+BAO, the middle panel is obtained for OHD+SNe+BAO and the right panel is obtained for OHD+SNe+BAO+CMBShift. The 1σ and 2σ confidence regions and the corresponding best fit curves (the central dark line) are shown.

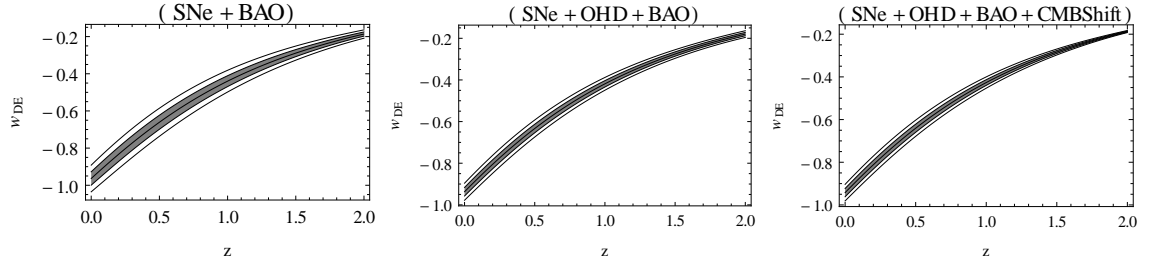


Figure 13. The plots of dark energy equation of state parameter $w_{DE}(z)$ for Model III. The left panel is obtained for SNe+BAO, the middle panel is obtained for OHD+SNe+BAO and the right panel is obtained for OHD+SNe+BAO+CMBShift. The 1σ and 2σ confidence regions and the corresponding best fit curves (the central dark line) are shown.

OHD, SNe, BAO and CMB shift parameter data (table 2, table 3 and table 4) shows that AIC or BIC can hardly reveal any significant information regarding the selection of model among these three. So, it is useful to introduce the Bayesian evidence for model selection. The Bayesian evidence is defined as,

$$E = \int (Prior \times Likelihood) d\theta_1 d\theta_2, \quad (5.3)$$

where θ_1 and θ_2 are the parameters of the model considered. In the present analysis, constant prior has been assumed for the parameter values for which the posterior is proportional to the likelihood. The evidence calculated for these two models are,

$$Model I : E_1 = P_1 \int Likelihood.dq_1 dq_2 = 5.134 \times 10^{-14}, \quad (5.4)$$

$$Model II : E_2 = P_2 \int Likelihood.dq_1 dq_2 = 7.773 \times 10^{-14}, \quad (5.5)$$

$$Model III : E_3 = P_3 \int Likelihood.dq_1 dq_2 = 21.79 \times 10^{-14}, \quad (5.6)$$

where P_1 , P_2 and P_3 are the constant prior of Model I, Model II and Model III respectively. The calculation of Bayesian evidence also does not give any significant information about the model selection as the value of E_1 , E_2 and E_3 are not significantly different. It can only be concluded that the Model III is marginally preferred than other two models.

6 Discussion

The present work is an attempt to reconstruct the interaction rate for holographic dark energy. The models, discussed in this paper, are based on the parameterizations of the deceleration parameter $q(z)$. The expressions of the Hubble parameter obtained for these parameterizations of the deceleration parameter (equation (2.17), (2.18) and (2.19)) give absolutely no indication to identify the dark matter and the dark energy components. The idea of the present work is to study the nature of interaction, mainly the interaction rate, for these three case assuming the dark energy to be holographic with Hubble horizon as the IR cut-off. As mentioned earlier, the holographic dark energy with Hubble horizon as the IR cut-off requires an interaction between dark energy and dark matter to generated the late time acceleration along with the matter dominated phase that prevailed in the past.

It has also been mentioned earlier that in a spatially flat geometry, the ratio of dark matter and dark energy density in a holographic dark energy model with Hubble horizon as the IR cut-off remains constant. Thus it could be a reasonable answer to the cosmic coincidence problem. As the dark energy equation of state parameter tends to zero at high redshift, the dark energy behaved like dust matter in the past. Thus it produces the matter dominated phase in the past which is consistent with the standard models of structure formation. The interaction rate (Γ) and consequently the interaction term Q , where $Q = \rho_H \Gamma$, remain positive through the evolution for the reconstructed models. It indicates that in the interaction, the energy transfers from dark energy to dark matter which is consistent with the second law of thermodynamics [104]. Though the parametrizations are different, the basic nature of interaction rate remains same in all the cases. Similar results have also been found by Sen and Pavon [87] where the interaction rate has been reconstructed from parametrization of dark energy equation of state. The dark energy equation of state parameter shows a highly phantom nature at present for the Model I and Model II. For Model III, it is inclined towards the non-phantom nature.

The plots of interaction rate for these models (figure 8, figure 9 and figure 10) show that the best fit curves for Model I and Model II behave in a very similar way and for Model III it is slightly different. The nature of the associated uncertainty is different for these three models. For Model II, the uncertainty increases at high redshift. Similar behaviour can also be found in the dark energy equation of state parameter ($w_{DE}(z)$) plots of the models (figure 11, figure 12 and figure 13).

In the present work, three different combinations of the data sets have been used in the analysis. The first one is the combination of SNe and BAO, the second combination is of OHD, SNe and BAO. The CMB shift parameter data has been added to it in the third combination. It is apparently clear that the addition of CMB shift parameter data does not lead to much improvement to the constraints on the model parameters. In case of the supernova data, the systematics have also been taken into account in the statistical analysis as the systematics might have its signature on the results. Some recent discussions on the effect of supernova systematics are discussed in [107–109].

For a comparison of models, different information criteria (namely the AIC and BIC) and the Bayesian evidence have been invoked. The Bayesian evidences calculated, are also of the same order of magnitude. It can only be concluded looking at the ratio of the Bayesian evidences of these three models that Mode III is slightly preferred than Model I and Model II, but they are comparable to each other in case of model selection.

Acknowledgments

The author would like to thank Professor Narayan Banerjee for guidance and valuable discussions. The author would also like to thank the anonymous referee, whose suggestions led to a substantial improvement of the paper.

References

- [1] A. G. Riess *et al.*, *Observational Evidence from Supernovae for an Accelerating Universe and a Cosmological Constant*, *Astron. J.* **116**, 1009 (1998).
- [2] S. Perlmutter *et al.*, *Measurements of Omega and Lambda from 42 High-Redshift Supernovae*, *Astrophys. J.* **517**, 565 (1999).
- [3] D. Schlegel, M. White, and D. Eisenstein, *The Baryon Oscillation Spectroscopic Survey: Precision measurements of the absolute cosmic distance scale*, arXiv:0902.4680 [astro-ph.CO].
- [4] N. Suzuki *et al.*, *The Hubble Space Telescope Cluster Supernova Survey: V. Improving the Dark Energy Constraints Above $z > 1$ and Building an Early-Type-Hosted Supernova Sample*, *Astrophys. J.* **746**, 85 (2012).
- [5] M. Crocce *et al.*, *Galaxy clustering, photometric redshifts and diagnosis of systematics in the DES Science Verification data*, *Mon. Not. R. Astron. Soc.* **455**, 4301 (2016).
- [6] S. Alam *et al.*, *The Eleventh and Twelfth Data Releases of the Sloan Digital Sky Survey: Final Data from SDSS-III*, *Astrophys. J. Suppl. Series* **219**, 12 (2015).
- [7] G. Hinshaw *et al.*, *Nine-Year Wilkinson Microwave Anisotropy Probe (WMAP) Observations: Cosmological Parameter Results*, *Astrophys. J.*, **208**, 19 (2013);
- [8] P. A. R. Ade *et al.* (Planck Collaboration), *Planck 2015 results. XIII. Cosmological parameters*, *Astron. Astrophys.* 594, A13 (2016).
- [9] S. Capozziello, S. Carloni and A. Troisi, *Quintessence without scalar fields*, *Recent Res. Dev. Astron. Astrophys.* **1**, 625 (2003), [astro-ph/0303041 (2003)].
- [10] S. M. Carroll, V. Duvvuri, M. Trodden and M. S. Turner, *Is cosmic speed-up due to new gravitational physics?*, *Phys. Rev. D* **70**, 043528 (2004).

- [11] D. N. Vollick, *1/R curvature corrections as the source of the cosmological acceleration*, Phys. Rev. D **68**, 063510 (2003).
- [12] S. Nojiri and S. D. Odintsov, *Modified gravity with negative and positive powers of curvature: Unification of inflation and cosmic acceleration*, Phys. Rev. D **68**, 123512 (2003).
- [13] S. M. Carroll *et al.*, *Cosmology of generalized modified gravity models*, Phys. Rev. D **71**, 063513 (2005).
- [14] O. Mena, J. Santiago and J. Weller, *Constraining Inverse-Curvature Gravity with Supernovae*, Phys. Rev. Lett., **96**, 041103 (2006).
- [15] S. Nojiri and S. D. Odintsov, *Modified $f(R)$ gravity consistent with realistic cosmology: From a matter dominated epoch to a dark energy universe*, Phys. Rev. D **74**, 086005 (2006).
- [16] S. Das, N. Banerjee and N. Dadhich, *Curvature-driven acceleration: a utopia or a reality?*, Classical Quantum Gravity **23**, 4159 (2006).
- [17] S. Nojiri and S. D. Odintsov, *Cosmological reconstruction of realistic modified $F(R)$ gravities*, Phys. Lett. B **681**, 74 (2009).
- [18] O. Bertolami and P. J. Martins, *Nonminimal coupling and quintessence*, Phys. Rev. D **61**, 064007 (2000).
- [19] N. Banerjee and D. Pavon, *A quintessence scalar field in Brans-Dicke theory*, Class. Quantum Grav. **18**, 593 (2001).
- [20] N. Banerjee and D. Paovn, *Cosmic acceleration without quintessence*, Phys. Rev. D **63**, 043504 (2001).
- [21] S. Sen and A. A. Sen, *Late time acceleration in Brans-Dicke cosmology*, Phys. Rev. D **63**, 124006 (2001).
- [22] D. F. Mota and J. D. Barrow, *Local and global variations of the fine-structure constant*, Mon. Not. R. Astron. Soc. **349**, 291 (2004).
- [23] D. F. Mota and J. D. Barrow, *Varying alpha in a more realistic universe*, Phys. Lett. B **581**, 141 (2004).
- [24] S. Das and N. Banerjee, *Brans-Dicke scalar field as a chameleon*, Phys. Rev. D **78**, 043512 (2008).
- [25] C. Deffayet, G. R. Dvali and G. Gabadadze, *Accelerated universe from gravity leaking to extra dimensions*, Phys. Rev. D **65**, 044023 (2002).
- [26] C. Deffayet, S. J. Landau, J. Raux, M. Zaldarriaga and P. Astier, *Supernovae, CMB, and gravitational leakage into extra dimensions*, Phys. Rev. D **66**, 024019 (2002).
- [27] S. Nojiri, S. D. Odintsov and M. Sami, *Dark energy cosmology from higher-order, string-inspired gravity, and its reconstruction*, Phys. Rev. D **74**, 046004 (2006).
- [28] G. R. Dvali, G. Gabadadze and M. Porrati, *4D gravity on a brane in 5D Minkowski space*, Phys. Lett. B **485**, 208 (2000).
- [29] M. W. Hossain, R. Myrzakulov, M. Sami and E. N. Saridakis, *Variable gravity: A suitable framework for quintessential inflation*, Phys. Rev. D **90**, 023512 (2014).
- [30] K. Bamba, Md. Wali Hossain, R. Myrzakulov, S. Nojiri and M. Sami, *Cosmological investigations of (extended) nonlinear massive gravity schemes with nonminimal coupling*, Phys. Rev. D **89**, 083518 (2014).
- [31] S. M. Carroll, *The Cosmological Constant*, Living Rev. Relativity **4**, 1 (2001).
- [32] T. Padmanabhan, *Cosmological Constant - the Weight of the Vacuum*, Phys. Rept. **380**, 235 (2003).
- [33] V. Sahni and A. A. Starobinsky, *The Case for a Positive Cosmological Lambda-term*, Int. J. Mod. Phys. D **9**, 373 (2000).
- [34] P. J. E. Peebles and B. Ratra, *The cosmological constant and dark energy*, Rev. Mod. Phys. **75**, 559 (2003).
- [35] E. J. Copeland, M. Sami and S. Tsujikawa, *Dynamics of dark energy*, Int. J. Mod. Phys. D **15**, 1753 (2006).

- [36] J. Martin, *Quintessence: a mini-review*, Mod. Phys. Lett. A **23**, 1252 (2008).
- [37] A. A. Starobinsky, *How to determine an effective potential for a variable cosmological term*, JETP Lett. **68**, 757 (1998), Pisma Zh. Eksp. Teor. Fiz. **68**, 721 (1998).
- [38] D. Huterer and M. S. Turner, *Prospects for probing the dark energy via supernova distance measurements*, Phys. Rev. D **60**, 081301 (1999);
- [39] D. Huterer and M. S. Turner, *Probing dark energy: Methods and strategies*, Phys. Rev. D **64**, 123527 (2001).
- [40] T. D. Saini, S. Raychaudhury, V. Sahini and A. A. Starobinsky, *Reconstructing the Cosmic Equation of State from Supernova Distances*, Phys. Rev. Lett. **85**, 1162 (2000).
- [41] J. Q. Xia, H. Li and X. Zhang, *Dark energy constraints after the new Planck data*, Phys. Rev. D **88**, 063501 (2013).
- [42] D. K. Hazra, S. Majumder, S. Pal, S. Panda and A. A. Sen, *Post-Planck dark energy constraints*, Phys. Rev. D **91**, 083005 (2015).
- [43] T. Holsclaw *et al.*, *Nonparametric reconstruction of the dark energy equation of state from diverse data sets*, Phys. Rev. D **84**, 083501 (2011).
- [44] S. Desai and N. J. Poplawski, *Non-parametric reconstruction of an inflaton potential from Einstein-Cartan-Sciama-Kibble gravity with particle production*, Phys. Lett. B **755**, 183 (2016).
- [45] A. Mukherjee, *Acceleration of the universe: a reconstruction of the effective equation of state*, Mon. Not. R. Astron. Soc. **460**, 273 (2016).
- [46] R. Rapetti, S. W. Allen, M. A. Amin and R. D. Blandford, *A kinematical approach to dark energy studies*, Mon. Not. R. Astron. Soc. **375**, 1510 (2007).
- [47] O. Luongo, *Dark energy from a positive jerk parameter*, Mod. Phys. Lett. A **28**, 1350080 (2013).
- [48] Z.-X. Zhai, M.-J. Zhang, Z.-S. Zhang, X.-M. Liu and T.-J. Zhang, *Reconstruction and constraining of the jerk parameter from OHD and SNe Ia observations*, Phys. Lett. B **727**, 8 (2013).
- [49] A. Mukherjee and N. Banerjee, *Parametric reconstruction of the cosmological jerk from diverse observational data sets*, Phys. Rev. D **93**, 043002 (2016).
- [50] S. Das, P. S. Corasaniti and J. Khoury, *Superacceleration as the signature of a dark sector interaction*, Phys. Rev. D **73**, 083509 (2006).
- [51] L. Amendola, M. Gasperini and F. Piazza, *Supernova Legacy Survey data are consistent with acceleration at $z \approx 3$* , Phys. Rev. D **74**, 127302 (2006).
- [52] L. Amendola, *Coupled quintessence*, Phys. Rev. D **62**, 043511 (2000).
- [53] L. Amendola, *Perturbations in a coupled scalar field cosmology*, Mon. Not. R. Astron. Soc. **312**, 521 (2000).
- [54] A. P. Billyard and A. A. Coles, *Interactions in scalar field cosmology*, Phys. Rev. D **61**, 083503 (2000).
- [55] W. Zimdahl, D. Pavon and L. P. Chimento, *Interacting Quintessence*, Phys. Lett. B **521**, 133 (2001).
- [56] L. Amendola and C. Quercellini, *Tracking and coupled dark energy as seen by the Wilkinson Microwave Anisotropy Probe*, Phys. Rev. D **68**, 023514 (2003).
- [57] R. Herrera, D. Pavon and W. Zimdahl, *Exact Solutions for the Interacting Tachyonic Dark Matter System*, Gen. Relativity Gravity **36**, 2161 (2004).
- [58] N. Banerjee and S. Das, Mod. Phys. Lett. A **21**, 2663 (2003).
- [59] A. Paliathanasis and M. Tsamparlis, *Two scalar field cosmology: Conservation laws and exact solutions*, Phys. Rev. D **90**, 043529 (2014).
- [60] S. Pan, S. Bhattacharaya and S. Chakraborty, *An analytic model for interacting dark energy and its observational constraints*, Mon. Not. R. Astron. Soc. **452**, 3038 (2015).

- [61] R. C. Nunes, S. Pan and E. Saridakis, *New constraints on interacting dark energy from cosmic chronometers*, Phys. Rev. D **94**, 023508 (2016).
- [62] R. Murgia, S. Gariazzo and N. Fornengo, *Constraints on Coupling between Dark Energy and Dark Matter from CMB data*, JCAP **04**(2016)014.
- [63] V. Salvatelli, N. Said, M. Bruni, A. Melchiorri and D. Wands, *Indication of late-time interaction in dark sector*, Phys. Rev. Lett. **113**, 181301 (2014).
- [64] T. Yang, Z.-K. Guo and R.-G. Cai, *Reconstructing the interaction between dark energy and dark matter using Gaussian processes*, Phys. Rev. D **91**, 123533 (2015).
- [65] B. Wang, E. Abdalla, F. Atrio-Barandela and D. Pavon, *Dark matter and dark energy interactions: theoretical challenges, cosmological implications and observational signatures*, Rept. Prog. Phys. **79**, 096901 (2016).
- [66] G. T. Hooft, *Dimensional Reduction in Quantum Gravity*, arXiv:gr-qc/9310026 (1993).
- [67] L. Susskind, *The world as a hologram*, J. Math. Phys. **36**, 6377 (1995).
- [68] J. D. Bekenstein, *Entropy bounds and black hole remnants*, Phys. Rev. D **49**, 1912 (1994).
- [69] A. Cohen, D. Kaplan and A. Nelson, *Effective Field Theory, Black Holes, and the Cosmological Constant*, Phys. Rev. Lett. **82**, 4971 (1999).
- [70] M. Li, *A Model of Holographic Dark Energy*, Phys. Lett. B **603**, 1 (2004).
- [71] W. Fischler and L. Susskind, *Holography and Cosmology*, arXiv:hep-th/9806039 (1998).
- [72] M. Cataldo, N. Cruz, S. del Campo and S. Lepe, *Holographic principle and the dominant energy condition for Kasner type metrics*, Phys. Lett. B **509** 138 (2001).
- [73] B. Guberina, R. Horvat and H. Nikolic, *Generalized holographic dark energy and the IR cutoff problem*, Phys. Rev. D **72** 125011 (2005).
- [74] B. Wang, Y. Gong and E. Abdalla, *Transition of the dark energy equation of state in an interacting holographic dark energy model*, Phys. Lett. B **624**, 141 (2005).
- [75] Q.-G. Huang and M. Li, *The holographic dark energy in a non-flat universe*, JCAP **08**(2004)013;
- [76] Y. Gong, B. Wang and Y.-Z. Zhang, *Holographic dark energy reexamined*, Phys. Rev. D **72**, 043510 (2005);
- [77] S. Nojiri and S. D. Odintsov, *Unifying phantom inflation with late-time acceleration: scalar phantom - non-phantom transition model and generalized holographic dark energy*, Gen. Relativity Gravity **38**, 1285 (2006);
- [78] B. Wang, C.-Y. Lin and E. Abdalla, *Constraints on the interacting holographic dark energy model*, Phys. Lett. B **637**, 357 (2006).
- [79] D. Pavon and W. Zimdahl, *Holographic dark energy and cosmic coincidence*, Phys. Lett. B **628**, 206 (2005);
- [80] W. Zimdahl and D. Pavon, *Interacting holographic dark energy*, Classical Quantum Gravity **24**, 5461 (2007).
- [81] N. Banerjee and D. Pavon, *Holographic dark energy in Brans-Dicke theory*, Phys. Lett. B **647**, 477 (2007).
- [82] L. Xu, *Holographic dark energy model with Hubble horizon as an IR cut-off*, JCAP09(2009)016.
- [83] S. del Campo, J. C. Fabris, R. Herrera and W. Zimdahl, *Holographic dark-energy models*, Phys. Rev. D **83**, 123006 (2011).
- [84] Y. Hu, M. Li, N. Li and Z. Zhang, *Holographic Dark Energy with Cosmological Constant*, JCAP **08**(2015)012.

- [85] R. C. G. Landim, *Holographic dark energy from minimal supergravity*, Int. J. Mod. Phys. D **25**, 165005 (2016).
- [86] N. Banerjee and N. Roy, *Stability analysis of a holographic dark energy model*, Gen. Relativity Gravity **47**, 92 (2015).
- [87] A. A. Sen and D. Pavon, *Reconstructing the interaction rate in holographic models of dark energy*, Phys. Lett. B **664**, 7 (2008).
- [88] P. A. R. Ade *et al.* (Planck Collaboration), *Planck 2013 results. XVI. Cosmological parameters*, Astron. Astrophys. **571**, A16 (2014).
- [89] Y. G. Gong and A. Wang, *Observational constraints on the acceleration of the Universe*, Phys. Rev. D **73**, 083506 (2006).
- [90] Y. G. Gong and A. Wang, *Reconstruction of the deceleration parameter and the equation of state of dark energy*, Phys. Rev. D **75**, 043520 (2007).
- [91] S. del Campo, I. Duran, R. Herrera and D. Pavon, *Three thermodynamically based parameterizations of the deceleration parameter*, Phys. Rev. D **86**, 083509 (2012).
- [92] J. Simon, L. Verde and R. Jimenez, *Constraints on the redshift dependence of the dark energy potential*, Phys. Rev. D **71**, 123001 (2005).
- [93] D. Stern, R. Jimenez, L. Verde, M. Kamionkowski and S. A. Stanford, *Cosmic chronometers: constraining the equation of state of dark energy. I: $H(z)$ measurements*, JCAP **02**(2010)008.
- [94] C.-H. Chuang and Y. Wang, *Modelling the anisotropic two-point galaxy correlation function on small scales and single-probe measurements of $H(z)$, $D_A(z)$ and $f(z)\sigma_8(z)$ from the Sloan Digital Sky Survey DR7 luminous red galaxies*, Mon. Not. R. Astron. Soc. **435**, 255 (2013).
- [95] M. Moresco, L. Verde, L. Pozzetti, R. Jimenez and A. Cimatti, *New constraints on cosmological parameters and neutrino properties using the expansion rate of the Universe to $z \sim 1.75$* , JCAP **07**(2012)053.
- [96] C. Blake *et al.*, *The WiggleZ Dark Energy Survey: joint measurements of the expansion and growth history at $z < 1$* , Mon. Not. R. Astron. Soc. **425**, 405 (2012).
- [97] C. Zhang, H. Zhang, S. Yuan, S. Liu, T.-J. Zhang and Y.-S. Sun, *Four new observational $H(z)$ data from luminous red galaxies in the Sloan Digital Sky Survey data release seven*, Res. Astron. Astrophys. **14**, 1221 (2014).
- [98] T. Delubac *et al.*, *Baryon acoustic oscillations in the $Ly\alpha$ forest of BOSS DR11 quasars*, Astron. Astrophys. **574**, A59 (2015).
- [99] M. Betoule *et al.*, *Improved cosmological constraints from a joint analysis of the SDSS-II and SNLS supernova samples*, Astron. Astrophys. **568**, A22 (2014).
- [100] O. Farooq, D. Mania and B. Ratra, *Hubble parameter measurement constraints on dark energy*, Astrophys. J., **764**, 138 (2013).
- [101] F. Beutler *et al.*, *The 6dF Galaxy Survey: baryon acoustic oscillations and the local Hubble constant*, Mon. Not. R. Astron. Soc. **416**, 3017 (2011).
- [102] L. Anderson *et al.*, *The clustering of galaxies in the SDSS-III Baryon Oscillation Spectroscopic Survey: baryon acoustic oscillations in the Data Releases 10 and 11 Galaxy samples*, Mon. Not. R. Astron. Soc. **441**, 24 (2014).
- [103] Y. Wang and S. Wang, *Distance Priors from Planck and Dark Energy Constraints from Current Data*, Phys. Rev. D **88**, 043522 (2013).
- [104] D. Pavon and B. Wang, *Le Chatelier-Braun principle in cosmological physics*, Gen. Relativity Gravity **41**, 1 (2009).

- [105] H. Akaike, *A New Look at the Statistical Model Identification*, IEEE Trans. Autom. Control **19**, 716 (1974).
- [106] G. Schwarz, *Estimating the Dimension of a Model*, Ann. Stat. **6**, 461 (1978).
- [107] S. Wang and Y. Wang, *Exploring the Systematic Uncertainties of Type Ia Supernovae as Cosmological Probes*, Phys. Rev. D **88**, 043511 (2013);
- [108] D. Rubin *et al.*, *UNITY: Confronting Supernova Cosmology's Statistical and Systematic Uncertainties in a Unified Bayesian Framework*, Astrophys. J. **813**, 137 (2015);
- [109] D. Shafer and D. Huterer, *Multiplicative errors in the galaxy power spectrum: self-calibration of unknown photometric systematics for precision cosmology*, Mon. Not. R. Astron. Soc. **447**, 2961 (2015).